AIAA-89-1146

An Acoustic Experimental and Theoretical Investigation of Single Disc Propellers

E. A. Bumann and K.D. Korkan
Texas A&M University, College Station, TX

AIAA 12th Aeroacoustics Conference
April 10–12, 1989 / San Antonio, TX

AN ACOUSTIC EXPERIMENTAL AND THEORETICAL INVESTIGATION OF SINGLE DISC PROPELLERS

A89-40478

Elizabeth A. Bumann*
Kenneth D. Korkan+

Texas A&M University
College Station, Texas 77843

Abstract

An experimental study of the acoustic field associated with two, three, and four blade propeller configurations with a blade root angle of 50° was performed in the Texas A&M University 5 ft. x 6 ft. acoustically insulated subsonic wind tunnel. A Waveform Analysis Package (WAVEPAK) was utilized to obtain experimental acoustic time histories, frequency spectra, and overall sound pressure level (OASPL) and served as a basis for comparison to the theoretical acoustic compact source theory of Succi. Valid for subsonic tip speeds, the acoustic analysis replaced each blade by an array of spiraling point sources which exhibited a unique force vector and volume. The computer analysis of Succi was modified to include a propeller performance strip analysis which used a NACA 4-digit series airfoil data bank to calculate lift and drag for each blade segment given the geometry and motion of the propeller. Theoretical OASPL predictions were found to moderately overpredict experimental values for all operating conditions and propeller configurations studied.

Nomenclature

a	=	Speed of sound.
c	=	Chord.
f(x,t)	=	Equation of solid surface of body in motion.
F_i	=	Net force of blade element on the fluid.
FFT	=	Fast Fourier Transform.
g	=	Equation of collasping sphere.
i	=	$\sqrt{-1}$.
ℓ_i	=	Aerodynamic force per unit area on the fluid at a body surface.
ℓ_r	=	Aerodynamic force per unit area acting on the fluid in the radiation direction.
M_r	=	Rotational Mach number.
n	=	Harmonic number.
p'	=	Acoustic pressure.
P	=	Instantaneous pressure at a point.
P_a	=	Pascal.
P_{ref}	=	Reference pressure (20 μPa).
P_{Lk}	=	Acoustic pressure due to loading.
P_{Tk}	=	Acoustic pressure due to thickness.
Q	=	Propeller torque.
r	=	Radial coordinate.
$\hat{r}_i$	=	Unit vector in the radiation direction.
t	=	Observer time.
T	=	Propeller thrust.
V_n	=	Velocity component normal to the body surface.
V_r	=	Velocity in the radiation direction.
x,y	=	Cartesian coordinates normal to the body surface.
δ	=	Dirac delta function.
ρ_∞	=	Free stream density.
τ	=	Source time.

Subscripts

ret	=	Retarded time.

Introduction

As fuel prices continue to fluctuate, many designers are showing renewed interest in propeller-driven aircraft. Conventional propeller configurations, due to their moderately low propulsive efficiencies at high speeds, were unable to compete with propulsion systems designed for low transonic flight regimes. Propellers at subsonic cruise speeds however, yield higher fuel efficiencies over other systems such as turbofans and turbojets. As a result, the aircraft industry has devoted substantial research toward the development of advanced propeller configurations capable of operating over a wide range of operating conditions.

The objective of this study is to present a theoretical and experimental study of the acoustic characteristics of single rotation propellers. In this study, two, three and four blade single disk propeller configurations have been tested at a blade root pitch angle of 40, 45, and 50° at an RPM range of 3500 to 7500 in increments of 250. The resulting experimental matrix serves as a basis for comparison of numerical noise predictions per Succi (1,2).

* Graduate Research Assistant, Department of Aerospace Engineering, AIAA Student Member.
+ Professor, Department of Aerospace Engineering, AIAA Associate Fellow.

Experimental Apparatus and Procedure

A counterrotating propeller test rig (3) (CRPTR) was used to study the nearfield acoustics of various single disc propeller configurations. Powered by an air turbine, the propeller disc was capable of producing a maximum of 55 horsepower at 16,000 RPM. Limitations, however, in the air supply allowed only 10 to 15 horsepower to be utilized. Although capable of operating in a counterrotation mode, the back disc of the CRPTR remained stationary with no blades attached for the single propeller disk testing.

With the use of the CRPTR, two, three, and four blade configurations were tested. Patterned after a commercially available aircraft propeller, the twenty inch diameter composite blades were modified in the shank region to force the thickness to chord ratio to be representative of a NACA 4-digit airfoil series shape with maximum camber located at mid-chord.

Construction of the composite blades (3) consisted of twenty five layers of unidirectional woven graphite cloth for thickness, one layer of bidirectional graphite cloth with fibers oriented at 45° to the propeller pitch change axis for torsional rigidity, and one layer of fiberglass cloth for surface finish on both the pitch and camber faces of the propeller. Experimental static tests of the blades in pure bending and axial loading indicated factors of safety in excess of six for each mode with no permanent deformation during loading and unloading cycles.

The open-return test section of the subsonic wind tunnel was acoustically insulated to obtain nearfield acoustic measurements. For easy restoration of the tunnel after testing, the acoustic treatment was fastened to a 0.75 inch plywood base in which one-quarter inch diameter wooden dowels were glued in streamwise rows. For high frequency absorption, a two inch layer of Dow Corning Type 701 fiberglass insulation was pressed over the sharpened pins. Next, a one inch sheet of four lb/ft^3 polystyrene material was installed for low frequency absorption. Using silicone caulking, styrofoam wedges of the same polystyrene material cut at 60° angles were fastened in a streamwise direction as shown in Figure 1. Four foot collection and diffusion sections were similarly constructed using wedges hot-wired to a 10° slope. Spanning a length of 24 feet, the acoustic insulation mounted to the walls, ceiling, and floor of the test section as shown in Figure 1, allowed a minimization of the reflective surroundings for fundamental acoustic measurements.

Two microphones, shown in Figure 2, were used to obtain the acoustic field for each blade configuration. The X-microphone, located at the reference plane midway between the fore and aft propeller disks in the counterrotating mode at a fixed distance of 1.625 inches from the propeller tip, was a B&K type 4134 pressure response 1/2 inch microphone. Located on axis with the CRPTR three inches from the spinner, the Y-microphone was a B&K 4133 free field 1/2 inch type. Each microphone was connected to a B&K type 2619 preamplifier with the complete acoustic instrumentation arrangement shown in Figure 3. To provide the necessary bias voltage to drive the microphones, the preamplifier was connected to a B&K type 2804 battery-driven power supply. Next, a B&K type 2203 OASPL meter was utilized to obtain overall sound pressure levels for the individual channels. From this, the acoustic signals from the microphones were passed into a filter box to remove the bias current from the B&K equipment. Finally, the digital data acquisition/reduction system, WAVEPAK (4), in conjunction with an IBM personal computer was connected to acquire both frequency and time domain acoustic information.

The WAVEPAK data acquisition program was used to acquire the acoustic time history and hence the spectral data from each microphone. The time history as well as a clear pattern of up to six harmonics over the broadband noise level shown in Figure 4, was observed for the X-microphone. The Y-microphone located forward of the spinner provided only an indication of the primary harmonic before being submerged in the tunnel broadband noise level. Similar spectra characteristics for the Y-microphone were measured for each blade configuration tested, consequently these data have not been included in this study.

Theoretical Procedure

Like other theoretical propeller acoustic formulations developed after the 1970's, the starting point for the acoustic compact source theory by Succi was the Ffwocs-Williams and Hawkings (5) (F-WH) equation without the quadrupole terms expressed as:

$$\frac{1}{a_\infty^2}\frac{\partial^2 p'}{\partial t^2} - \nabla^2 p' = \frac{\partial}{\partial t}\left[\rho_\infty v_n |\nabla f|\, \delta(f)\right] - \frac{\partial}{\partial x_i}\left[\ell_i |\nabla f|\, \delta(f)\right] \qquad (1)$$

Succi subdivided the propeller into small chordwise and spanwise sections. Summing the pressure of each section labeled by the subscript k, the acoustic pressure has been defined as:

$$P'(x,t) = \sum_k P_{Lk} + P_{Tk} \qquad (2)$$

where:

$$4\pi P_{Lk} = -\frac{\partial}{\partial x_i}\int_{S_k}\left[\frac{P_{ij}n_j}{r|1-M_r|}\right] dS_k \qquad (3)$$

$$4\pi P_{Tk} = \frac{\partial}{\partial t}\int_{S_k}\left[\frac{\rho_\infty V_n n_i}{r|1-M_r|}\right] dS_k \qquad (4)$$

P_{Lk} represents the pressure due to loading noise and P_{Tk} denotes the pressure due to thickness noise. Assume that the pressure forces on the interior surfaces of a segment are zero or cancel with their immediate neighbors. For small segments and thin blades, the integrals in Equations (3) and (4) can be evaluated as if the subsections were a compact or point source. Assuming that the pressure and speed of an element k are nearly constant as the sphere (g=0) moves across the sections, and if the maximum

dimension of the element is small relative to the distance from the observer, the loading noise component is written as:

$$4\pi P_L(x,t) = \left[\frac{1}{r(1-M_r)^2}\left[\frac{\vec{r}_i}{a_\infty}\frac{\partial f_i}{\partial \tau} + \frac{F_i\vec{r}_i}{(1-M_r)}\left(\frac{\vec{r}_i}{a_\infty}\frac{\partial M_i}{\partial \tau}\right)\right]\right.$$

$$\left. + \frac{1}{r^2(1-M_r)^2}\left[\vec{r}_i F_i\left(\frac{1-M_i^2}{1-M_r}\right) - F_i M_i\right]\right]_{ret} \qquad (5)$$

where:

$$M_i = \frac{(\partial y_i/\partial \tau)}{a_\infty}$$

$$M_r = \vec{r}_i M_i$$

F_i is the net force exerted on the medium due to the pressure on the surface S. Equation (5) is identical to the Lowson (6) result for sound radiation from a moving point source. The thickness noise component is developed from the volume associated with each segment. Define F as the intersection of the sphere with the body surface. If the source is compact, then the relative velocity with respect to the observer is the same for all segments. The effective volume, ψ, is therefore related to the actual volume, ψ_0, by the relation:

$$\psi = \int |A(r)|\,dr = \frac{1}{|1-M_r|}\int A(L)dL = \frac{\psi_0}{|1-M_r|}$$

where $dL = |1-M_r|dr$ and is an increment of length in a coordinate system fixed to the body. The effective volume is enclosed by F which changes with time due to the motion of the body. The thickness noise component is written as:

$$4\pi P_T(x,t) = \rho_\infty\left[\frac{1}{1-M_r}\frac{\partial}{\partial \tau}\left[\frac{1}{1-M_r}\right.\right.$$

$$\left.\left.\frac{\partial}{\partial \tau}\left[\frac{1}{1-M_r}\frac{\partial}{\partial \tau}\left(\frac{\psi_0}{r(1-M_r)}\right)\right]\right]\right]_{ret} \qquad (6)$$

where,

$$\frac{\partial}{\partial t} = \frac{1}{|1-M_r|}\frac{\partial}{\partial \tau}$$

$$\frac{\partial r}{\partial \tau} = -v_r$$

Both the loading and thickness noise as expressed in Equations (5) and (6) were placed into the numerical analysis of Succi. The aerodynamic performance characteristics of the blades however, were read from an input data file obtained by the separate propeller performance code.

The propeller strip analysis method used to estimate the aerodynamic forces along the blade span was developed by Cooper (7). Performance calculations are valid for subsonic tip velocities and advance ratios of approximately eight-tenths or greater for single rotation propellers using this analysis. Lift and drag coefficients as functions of radial location were calculated from a NACA 4-digit series airfoil data bank (8) to obtain thrust and torque forces along the blade. The aerodynamic forces, as well as the chord, thickness/chord ratio, and blade angle distribution were transformed into ninth order polynomials (9) to allow the user flexibility in the acoustic calculations with regard to grid variations. The polynomials were written in the form:

$$(dT/d(\tfrac{x}{c}))/T = a_9 + b_9(\tfrac{x}{c}) + c_9(\tfrac{x}{c})^2 + \ldots + h_9(\tfrac{x}{c})^9 \qquad (7)$$

$$(dQ_F/d(\tfrac{x}{c}))/Q_F = a_9 + b_9(\tfrac{x}{c}) + c_9(\tfrac{x}{c})^2 + \ldots + h_9(\tfrac{x}{c})^9 \qquad (8)$$

where $(dT/d(\frac{x}{c}))/T$ represents the radial thrust distribution and $(dQ_F/d(\frac{x}{c}))/Q_F$ is the torque radial distribution corresponding to a radial value of x/c. The numerical analysis developed in this study incorporated the strip analysis to calculate propeller performance values and was utilized directly in the Succi compact acoustic source method predictions.

Results

A source may be considered compact if the differences in path length from all points along the blade to an observer are small compared to a typical wavelength of the sound generated. To ensure that this assumption had not been violated, several mesh sizes were examined (10) for the twenty inch diameter propeller under study. Chordwise and spanwise variations along the blade ranged from a course grid consisting of 5 points from hub to tip to a fine mesh size of 100 points. The frequencies associated with each blade configuration ranged from 200 to 7024 Hz. Although the blades were modeled differently, each grid examined satisfied the compact source assumption.

Performance calculations for an RPM range between 400 and 7500 yielded acceptable performance values for the experimental composite propeller design. For example, the two blade 50° blade set configuration resulted in propeller efficiencies from 0.72 to 0.84. For a range of advance ratios between 0.71 and 1.01, total propeller thrust values of 9 to 25 lbs with corresponding torque values of 4 to 8 ft.-lbs. were computed (10).

Comparison between theoretical and experimental values of OASPL for the two blade configuration shown in figure 5, validated the compact source assumption. The prediction values by Succi appears to be linear, however a similar trend was also indicated by the experimental data. Better compliance between experimental and theoretical values would be indicated using a conservative data error band of ±2.5%. Acoustic comparisons in the frequency domain were evaluated for the first fifteen harmonics as shown in figures 6 and 7. Experimental SPL

values were calculated from the root-mean-square voltages obtained from the WAVEPAK FFT spectral analysis program using the expression:

$$SPL = 20 \log_{10} |P/P_{ref}| \qquad (9)$$

The measured pressure of the sound wave, P, was obtained by dividing the spectral analysis voltage values by the microphone sensitivity value taken as 0.116 V/Pa for the X-microphone. An error of ±3 Hz from the blade passing frequency was accepted for each harmonic. The OASPL was calculated by summing each harmonic until no noticeable difference occurred in the OASPL value, i.e., to the fourth decimal place. Only the first four harmonics were found to effect the magnitude of the OASPL value. Similar to the experimental method, theoretical SPL values were calculated from a Fourier analysis of the pressure time histories as predicted by Succi.

Comparisons in the frequency domain for a low and high advance ratio, shown in Figures 6 and 7, indicate a larger disagreement between experimental and theoretical values at the lower RPM. Also presented in these Figures are the theoretical acoustic time histories as predicted by the Succi analysis in terms of loading, thickness, and total noise components for each test condition. The acoustic analysis indicates that the blade is loading noise dominant in comparison to the magnitude of the thickness noise contribution. Therefore, the total acoustic time history is driven by the loading acoustic time history.

To investigate the variation of each of the components of the acoustics associated with the Succi analysis, a range of advance ratios was used to predict the acoustic time histories for thickness, loading, and total noise components. The loading acoustic component shown in Figure 8, increased dramatically by a factor of approximately four as the advance ratio went from 1.30 to 0.91, i.e., as RPM increased. The acoustic time histories for all advance ratio values, however, were of the same form. The magnitude of the thickness noise variation shown in Figure 9, in comparison to the loading noise reaffirmed that the propeller configuration was loading noise dominant. Since the acoustic analysis in Figures 8 and 9 had indicated that this propeller configuration was loading noise dominant, the total acoustic waveform shown in Figure 10 was similar to the individual loading noise acoustic time history.

Theoretical and experimental comparisons of OASPL values for a three blade propeller configuration shown in Figure 11, resulted in overprediction of the compact source theory. However when considering the ±2.5% data error band for experimental values, better agreement between theoretical and experimental OASPL values would exist. Similar to the two blade configuration, the theoretical prediction values appear to be linear.

Differences in the OASPL values for the theoretical and experimental methods can be attributed to discrepancies found in the frequency domain as shown in Figures 12 and 13. Recall that the magnitude of the OASPL depends on at least the first four harmonics where large SPL differences exist. Similar to the two blade case, the three blade configuration indicated loading noise dominance. An investigation of the loading, thickness, and total acoustic components as shown in Figures 14 through 16 indicated that again the total noise component of the acoustic time histories was driven by the loading acoustic time histories.

The same trends for OASPL as those seen for the two and three blade configurations are shown in Figure 17 for the four blade configuration. Comparisons between 2, 3, and 4 blade configurations has shown that as the number of blades increased, the OASPL decreased. The frequency spectra for low and high advance ratios for the four blade propeller configuration shown in Figures 18 and 19, indicated discrepancies between theoretical predictions and experimental values at the first four harmonics. The acoustic time histories associated with each test condition similar to the other blade arrangements, indicated that this configuration was loading dominant. Comparison of the magnitudes of the acoustic time histories for thickness, loading, and total noise components shown in Figures 20 through 22 reaffirmed the magnitude and influence of the loading noise contribution.

Summary/Conclusion

A study of the acoustic field associated with single disc propellers has been presented. Two, three, and four blade configurations at a blade root pitch angle of 50° were examined for a RPM range between 3500 and 7000 in increments of 250 and compared with theoretical predictions of the Succi numerical acoustic analysis. An acoustically insulated subsonic wind tunnel was used to obtain experimental acoustic data for a microphone located in the propeller disc plane. Time and frequency domain information was then found through the use of a digital data acquisition system known as WAVEPAK. Used in conjunction with an IBM PC, the WAVEPAK system provided a two channel oscilloscope and FFT analyzer.

Theoretical acoustic fields were modeled as an array of spiraling point sources. Each point was developed by subdividing the blades in both the chordwise and spanwise directions. Thrust and torque forces associated with each segment were theoretically calculated from a propeller performance strip analysis incorporated into the numerical acoustic prediction technique. A NACA 4-digit series airfoil data bank was used to obtain the lift and drag radial distributions along the blade.

The theoretical method of acoustic compact sources, as described in this study, provided reasonable results. Theoretical OASPL values overpredicted experimental values for all blade configurations tested. Differences, however, in the frequency spectra for approximately the first five harmonics did exist. Similar conclusions

were found by Bumann (10) at blade root angles of 40 and 45°. The lower theoretical values of SPL at the higher frequencies were associated with the intrusion of tunnel background or propeller test rig noise rather than true propeller noise. Examination of the acoustic time histories revealed that each blade configuration was loading noise dominant.

The numerical acoustic prediction analysis by Succi is general and can be applied to any propeller geometry and subsonic helical tip Mach number operating condition. Consequently, the acoustic radiation field associated with single disc propellers can be easily predicted given only the shape and motion of the propeller.

Acknowledgment

This research was sponsored by NASA Lewis Research Center Grant NAG 3-354. The authors would also like to acknowledge the assistance of Mr. J.A. Gazzaniga for providing the experimental data contained in this work.

References

1. Succi, G.P., "Design of Quiet Efficient Propellers," SAE Paper 790584, 1979.

2. Succi, G.P., Munro, D.H. and Zimmer, J.A., "Experimental Verification of Propeller Noise Prediction," AIAA Paper 80-0994, 1980.

3. Gazzaniga, J.A., "Acoustic Experimental Investigation of Counterrotating Propeller Configurations," Master of Science Thesis, Texas A&M University, August 1989.

4. Anonymous, "WAVEPAK-Users Manual," Computational Systems, Inc., Knoxville, Tennessee, 1986.

5. Ffwocs-Williams, J.E. and Hawkings, D.L., "Sound Generated by Turbulence and Surface in Arbitrary Motion," Phil, Trans. of the Roy. Aero. Society of London, Vol A264, 1969, pp. 321-342.

6. Lowson, M.V., "The Sound Field for Singularities in Motion," Proc. Roy. Soc. London, Vol. 286, 1965, pp. 559-572.

7. Cooper, J.P., "The Linearized Inflow Propeller Strip Analysis," WADC TR 65-615, 1957.

8. Korkan, K.D., Camba, J., and Morris, P.M., "Aerodynamic Data Banks for Clark-Y, NACA 4-Digit, and NACA 16-Series Airfoil Families," Aerospace Engineering Department, Texas A&M University, January 1986.

9. Dowty Rotol, Private Communication, 1988.

10. Bumann, E.A., "An Experimental and Theoretical Acoustic Investigation of Single Disc Propellers," Master of Science Thesis, Texas A&M University, December 1988.

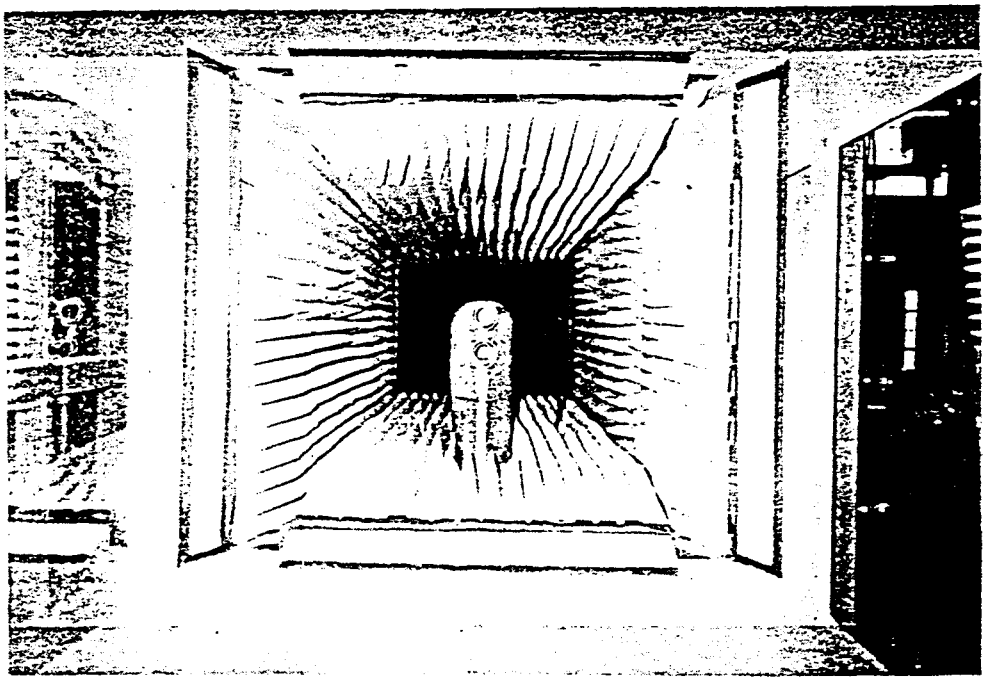

Figure 1. Acoustically Insulated Wind Tunnel.

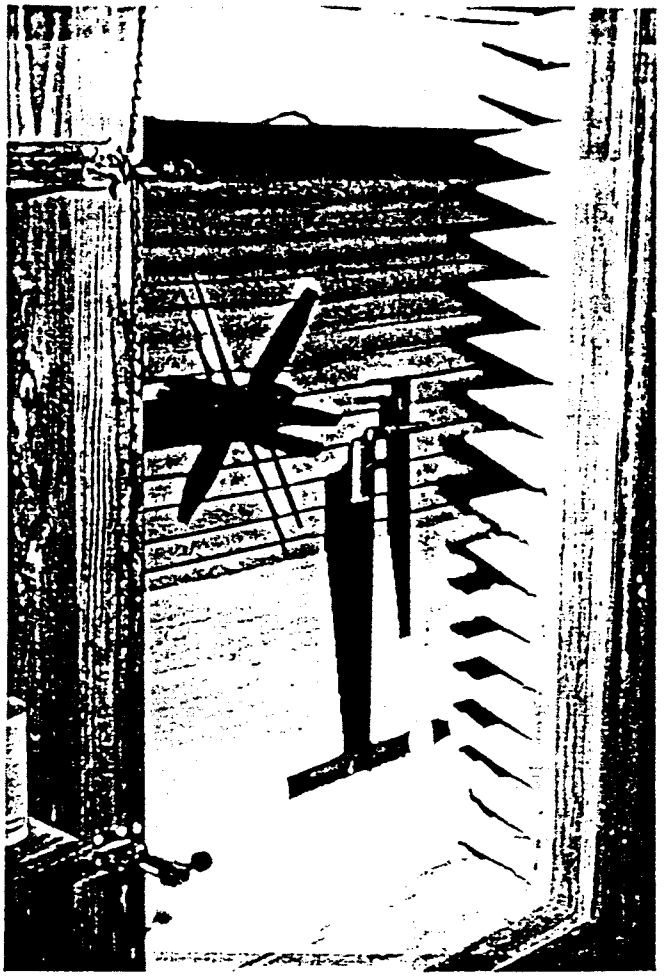

Figure 2. Microphone Location.

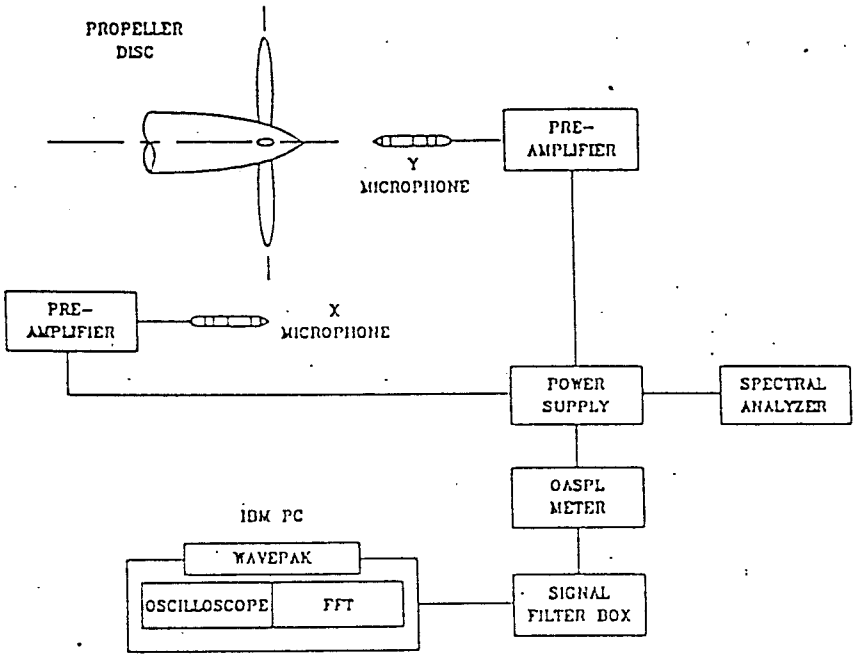

Figure 3. Schematic of Experimental Setup.

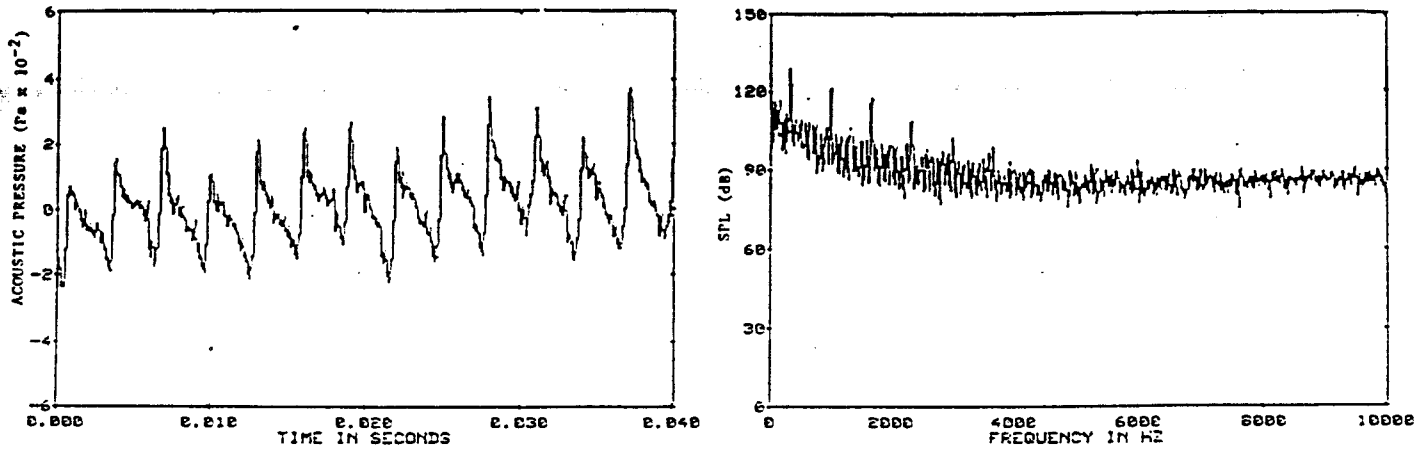

Figure 4. Experimental Acoustic Time History and Frequency Spectra (r/R = 1.081, 4 Blade, disc plane).

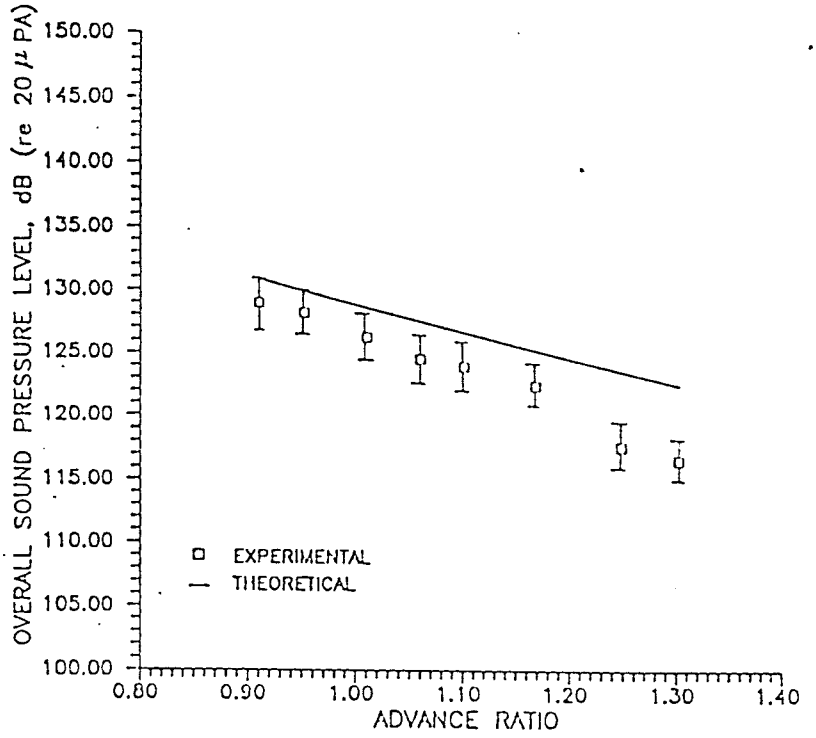

Figure 5. OASPL as a Function of Advance Ratio for a Two Blade 50° Propeller Configuration.

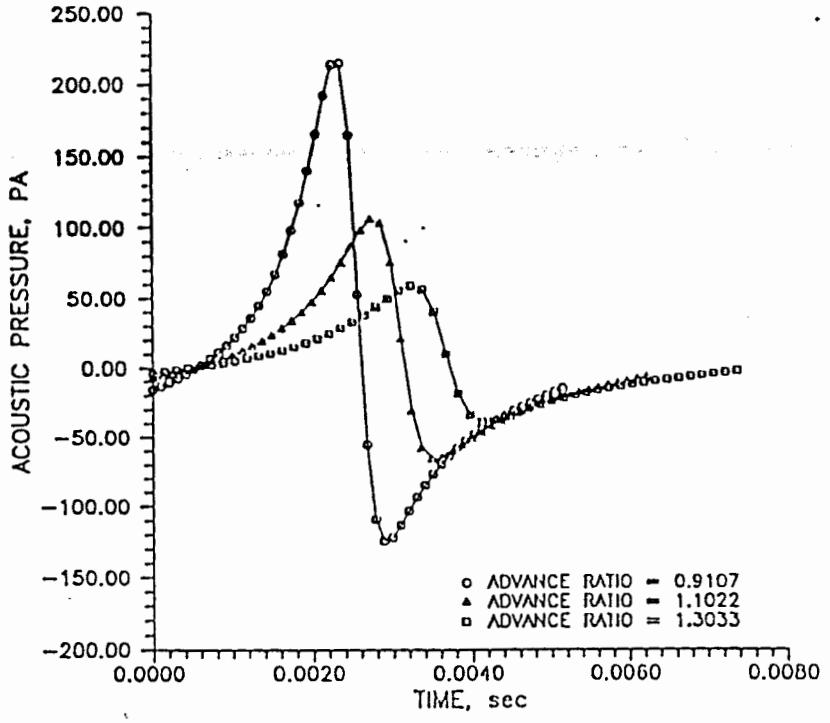

Figure 8. Loading Acoustic Time History Component for a Two Blade 50° Propeller Configuration.

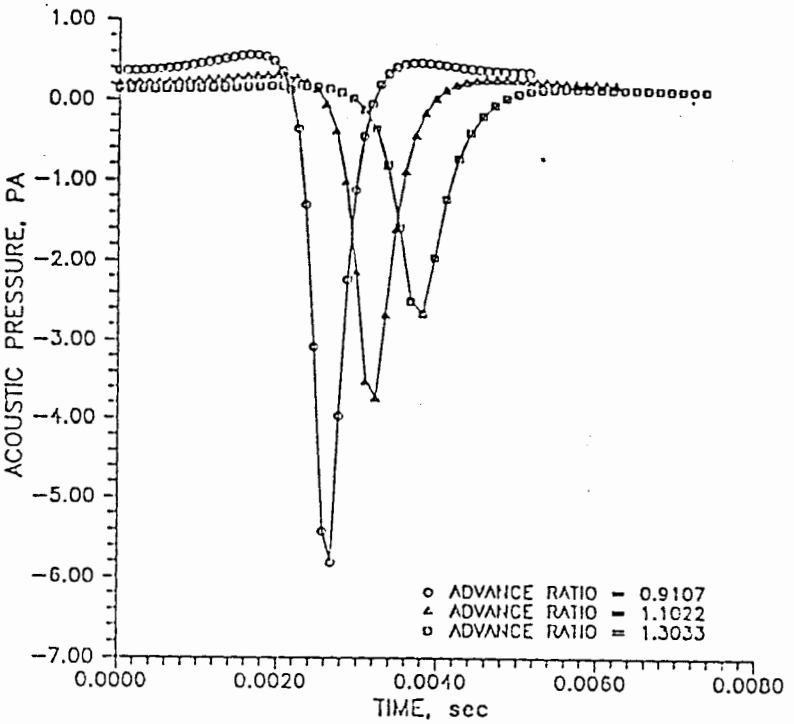

Figure 9. Thickness Acoustic Time History Component for a Two Blade 50° Propeller Configuration.

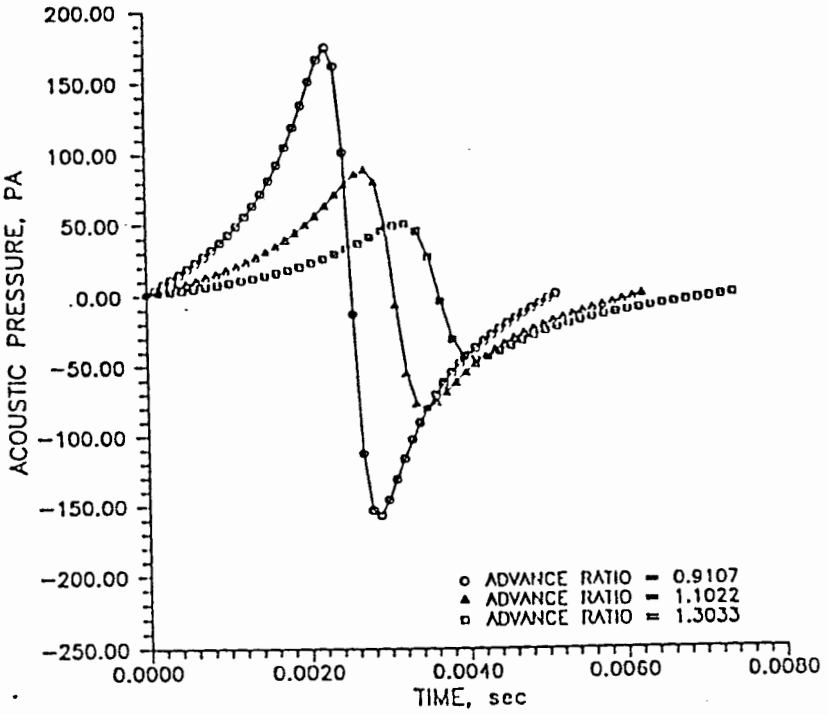

Figure 10. Total Acoustic Time History Component for a Two Blade 50° Propeller Configuration.

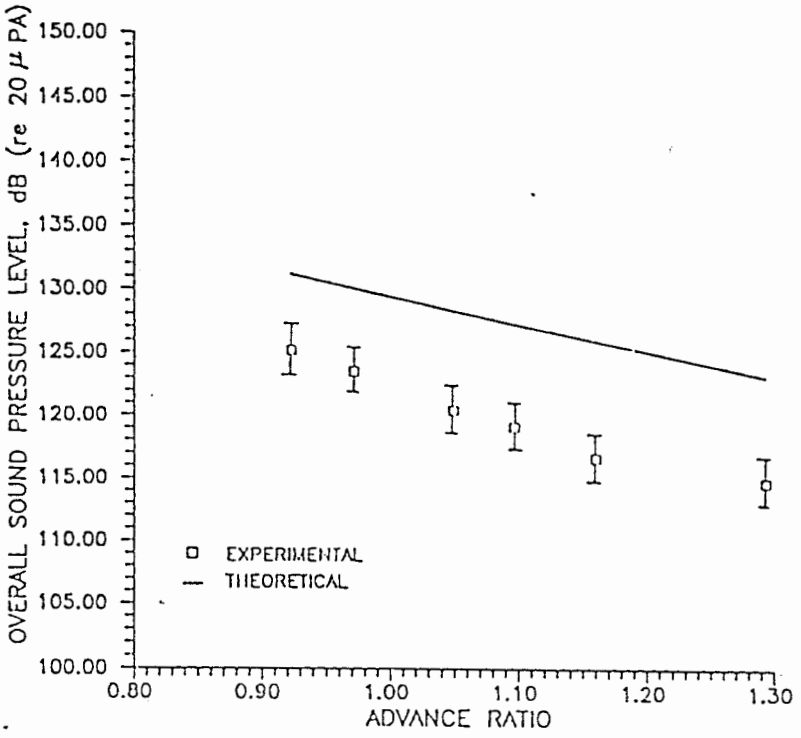

Figure 11. OASPL as a Function of Advance Ratio for a Three Blade 50° Propeller Configuration.

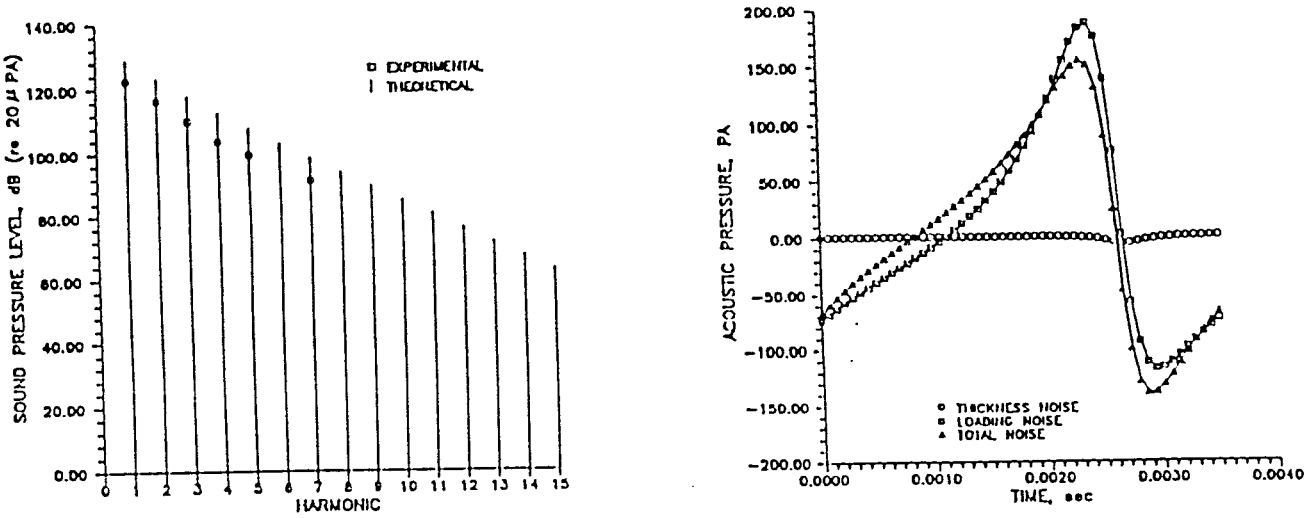

(a) (b)

Figure 12. Three Blade 50° Propeller Configuration at an Advance Ratio of 0.9716.
a) Frequency Spectra Comparisons
b) Theoretical Acoustic Time Histories

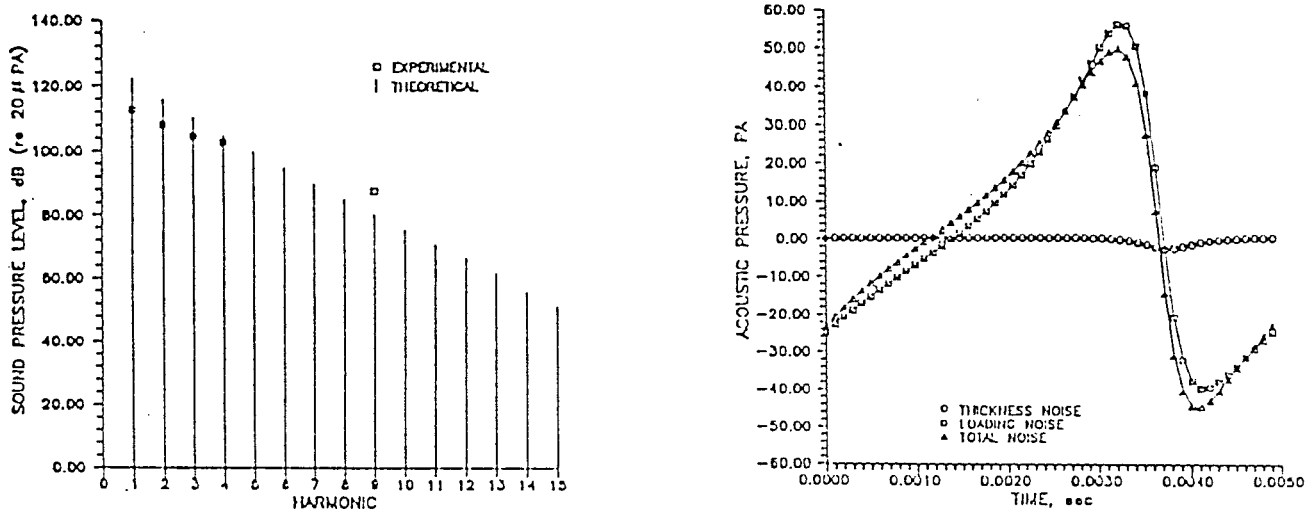

(a) (b)

Figure 13. Three Blade 50° Propeller Configuration at an Advance Ratio of 1.2936.
a) Frequency Spectra Comparisons
b) Theoretical Acoustic Time Histories

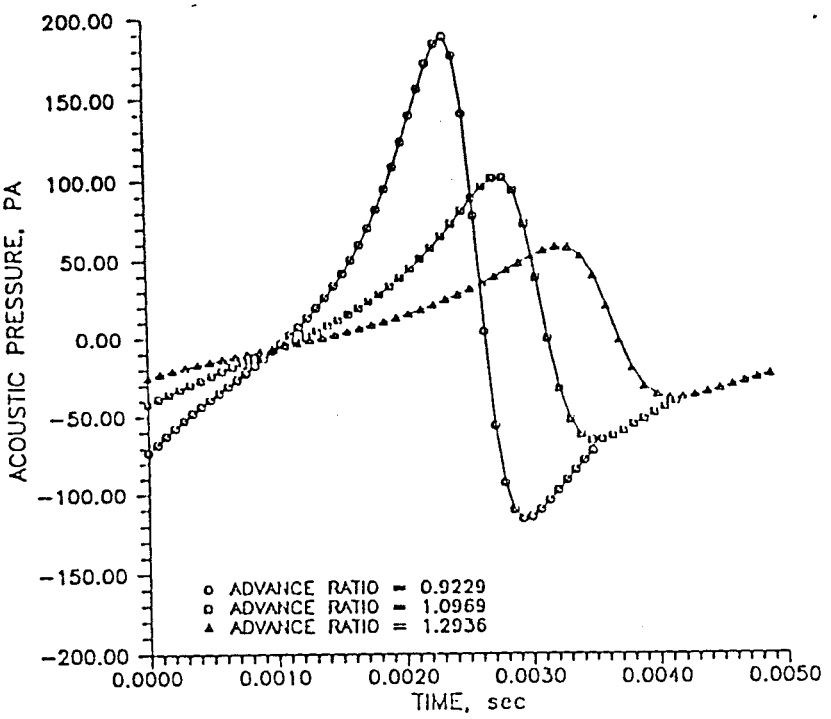

Figure 14. Loading Acoustic Time History Component for a Three Blade 50° Propeller Configuration.

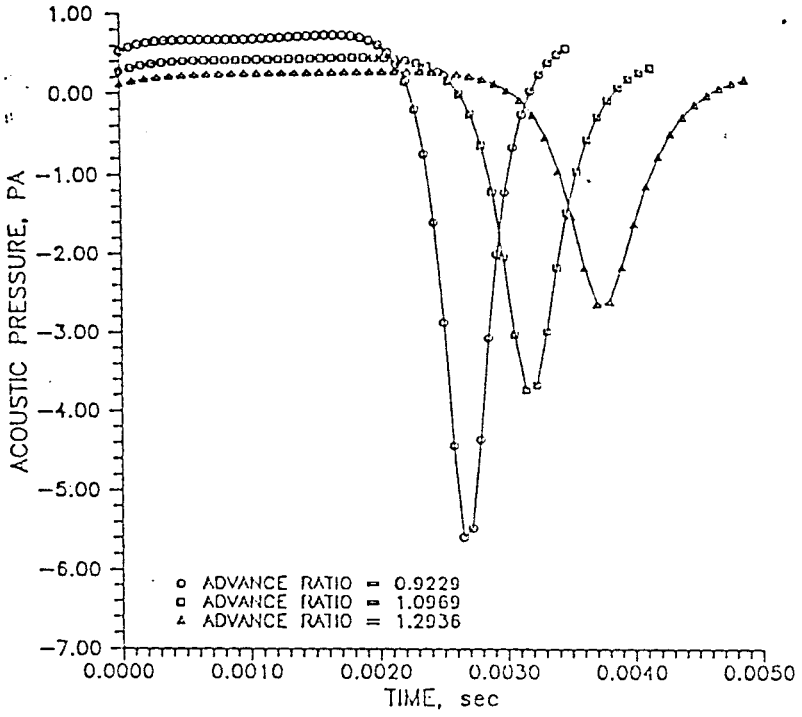

Figure 15. Thickness Acoustic Time History Component for a Three Blade 50° Propeller Configuration.

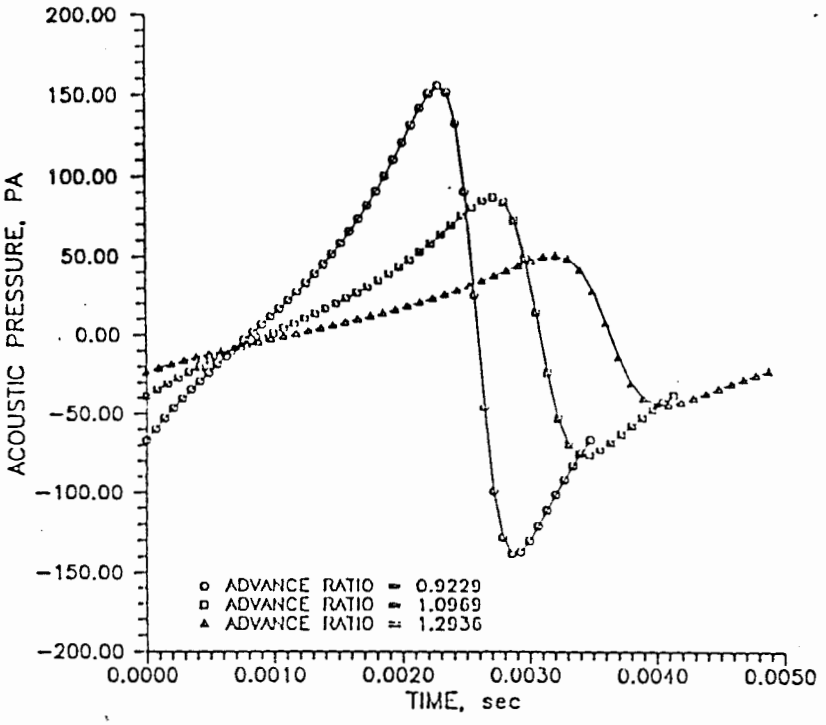

Figure 16. Total Acoustic Time History Component for a Three Blade 50° Propeller Configuration.

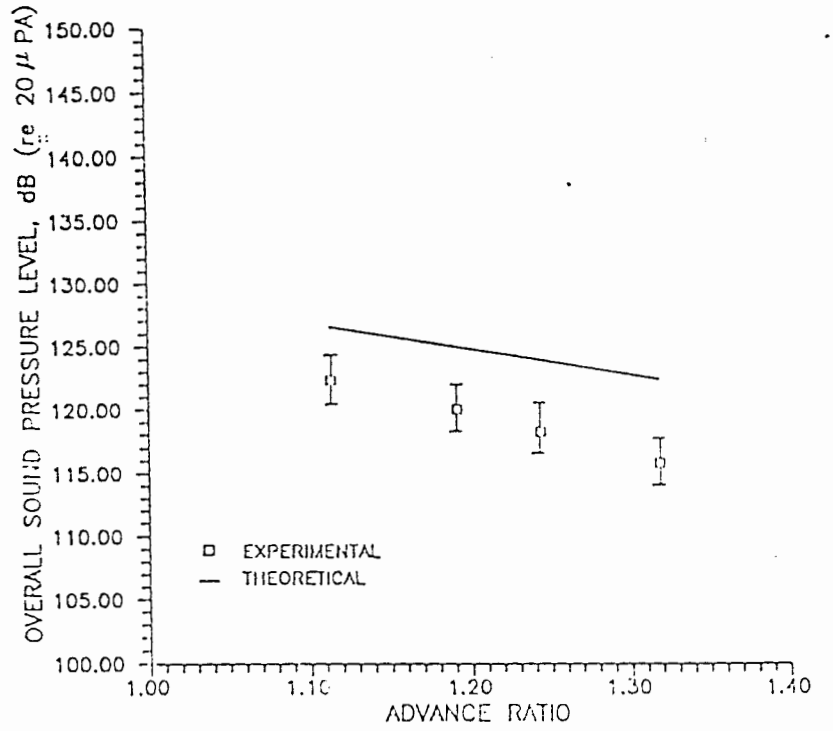

Figure 17. OASPL as a Function of Advance Ratio for a Four Blade 50° Propeller Configuration.

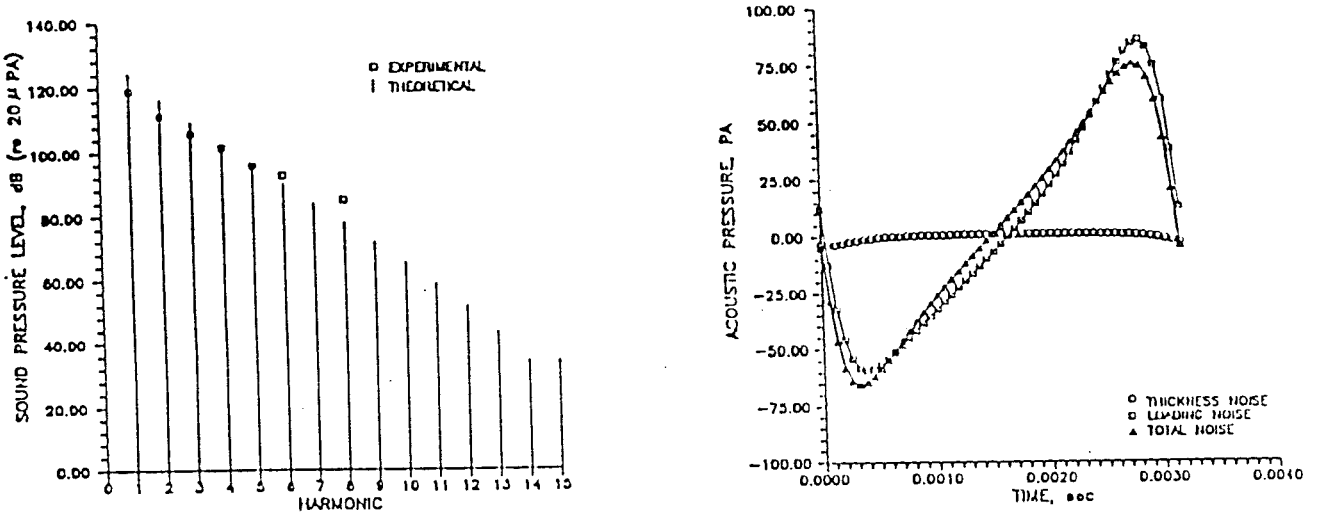

(a) (b)

Figure 18. Four Blade 50° Propeller Configuration at an Advance Ratio of 1.1916.
a) Frequency Spectra Comparisons
b) Theoretical Acoustic Time Histories

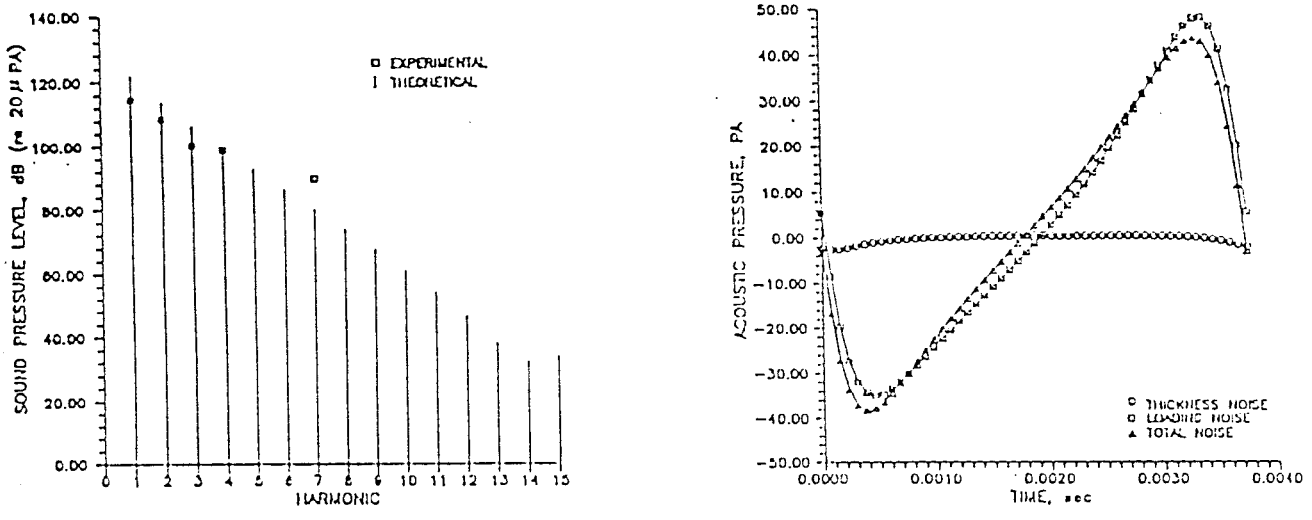

(a) (b)

Figure 19. Four Blade 50° Propeller Configuration at an Advance Ratio of 1.3184.
a) Frequency Spectra Comparisons
b) Theoretical Acoustic Time Histories

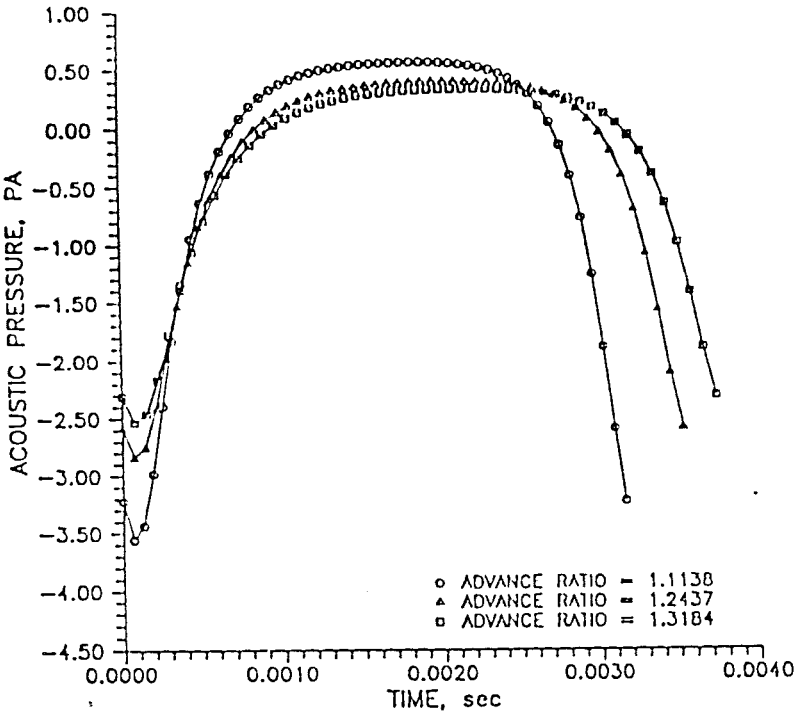

Figure 20. Thickness Acoustic Time History Component for a Four Blade 50° Propeller Configuration.

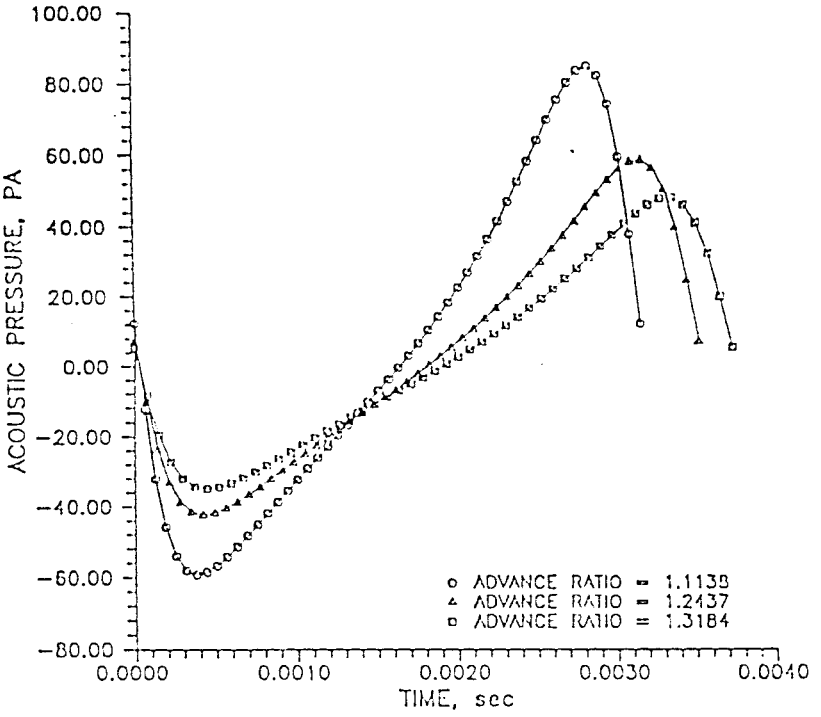

Figure 21. Loading Acoustic Time History Component for a Four Blade 50° Propeller Configuration.

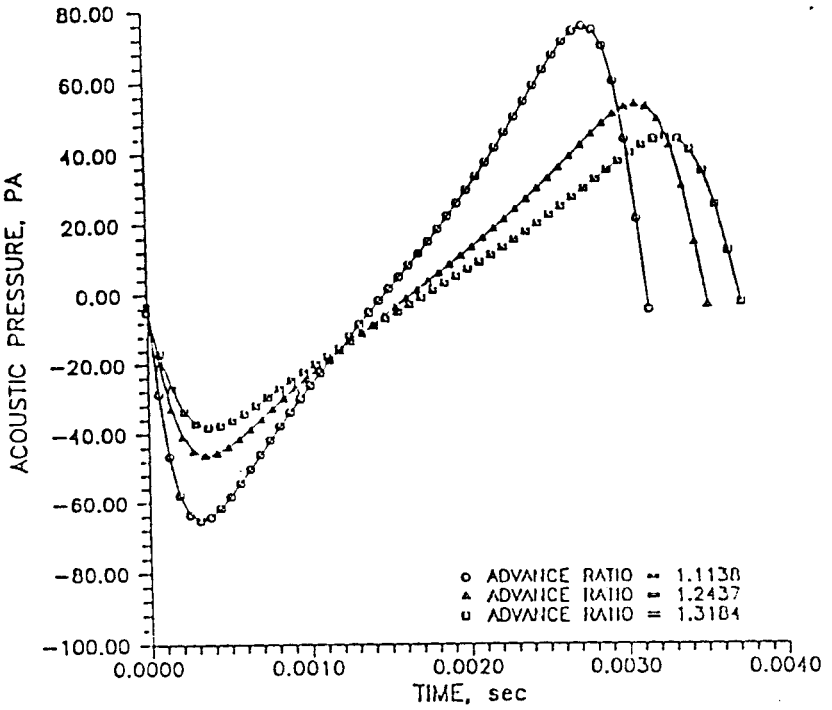

Figure 22. Total Acoustic Time History Component for a Four Blade 50° Propeller Configuration.